Scientific Reports

https://doi.org/10.1038/s41598-026-45469-2

Article in Press

TRIM29 promotes epithelial–mesenchymal transition, angiogenesis, and stromal remodeling in lung adenocarcinoma: integrated validation at histologic, transcriptomic, and protein levels

Received: 7 November 2025

Accepted: 19 March 2026

Published online: 22 March 2026

Cite this article as: Hwang Y., Han J., Haam S. *et al. TRIM29* promotes epithelial–mesenchymal transition, angiogenesis, and stromal remodeling in lung adenocarcinoma: integrated validation at histologic, transcriptomic, and protein levels. *Sci Rep* (2026). https://doi.org/10.1038/s41598-026-45469-2

Yoonjung Hwang, Jae-Ho Han, Seokjin Haam, Hyun Woo Lee & Young Wha Koh

TRIM29 Promotes Epithelial–Mesenchymal Transition, Angiogenesis, and Stromal Remodeling in lung adenocarcinoma: Integrated Validation at Histologic, Transcriptomic, and Protein Levels

Yoonjung Hwang[1], Jae-Ho Han, M.D. Ph.D.[1], Seokjin Haam, M.D, Ph.D.[2], Hyun Woo Lee, M.D.[3], Young Wha Koh, M.D, Ph.D.[1,4]

[1]Department of Pathology, Ajou University School of Medicine, Suwon-si, South Korea

[2]Department of Thoracic and Cardiovascular Surgery, Ajou University School of Medicine, Suwon-si, South Korea

[3]Department of Hematology-Oncology, Ajou University School of Medicine, Suwon-si, South Korea

[4]Department of Biomedical Science, Graduate School of Ajou University, Suwon, Republic of Korea.

***Corresponding author:**

Young Wha Koh, M.D., Ph.D. Professor, Department of Pathology, Ajou University School of Medicine, 206 Worldcup-ro, Yeongtong-gu, Suwon-si, Gyeonggi-do 16499, Republic of Korea

☎ +82-31-219-7055 (Fax) +82-31-219-5934 (E-mail) youngwha9556@gmail.com

Running title: *TRIM29* and lung adenocarcinoma

ABSTRACT

TRIM29 is implicated in cancer progression; however, its function in lung adenocarcinoma (LUAD) remains unknown. We assessed the contribution of *TRIM29* to LUAD biology, its influence on the tumor microenvironment (TME), and its prognostic relevance in LUAD. We analyzed two independent LUAD transcriptomic cohorts. Gene set enrichment analysis (GSEA) was performed using deconvolution-based TME profiling with xCell, ESTIMATE, and EPIC. Associations between *TRIM29* and epithelial–mesenchymal transition (EMT), angiogenesis, stromal remodeling, and survival were corroborated using immunohistochemistry, histopathology, and cell line assays. Drug sensitivity analyses were performed to identify therapeutic agents for *TRIM29*-high tumors. GSEA consistently showed enrichment of EMT in *TRIM29*-high tumors across both mRNA datasets. Deconvolution revealed that *TRIM29*-high tumors harbored an increased number of fibroblasts and endothelial cells, along with elevated stromal scores. The GSEA and deconvolution results using the *TRIM29*-associated transcriptional module were consistent with those obtained from the single-gene analysis. In an independent cohort, immunohistochemistry and histopathology confirmed positive correlations between TRIM29 expression and SNAIL, TWIST, microvessel density, and stromal

proportion. High TRIM29 expression at the transcript and protein levels is associated with poor overall survival. Functionally, TRIM29 inhibition in cell lines decreased N-cadherin, SNAIL, and TWIST expression while increasing E-cadherin expression. Drug response profiling revealed that mTOR inhibitors exhibited the highest activity in *TRIM29*-high cells. To our knowledge, this study provides evidence suggesting that *TRIM29* may be associated with EMT-related transcriptional programs, angiogenesis, and stromal remodeling in LUAD, as well as with adverse clinical outcomes. An integrated pathology-transcriptome-outcome framework supports biomarker-guided strategies for *TRIM29*-high tumors, with mTOR inhibition emerging as a promising therapeutic strategy.

KEYWORDS: lung adenocarcinoma; *TRIM29*; epithelial-mesenchymal transition; angiogenesis; stromal remodeling

Introduction

Lung cancer is one of the leading causes of death worldwide, and non-small cell lung cancer (NSCLC) accounts for approximately 85% of all cases(1). Lung adenocarcinoma (LUAD) is the most common subtype of lung cancer. Although LUAD has a poor prognosis, recent advancements in targeted therapies, such as tyrosine kinase inhibitors and immunotherapies, such as immune checkpoint inhibitors, have significantly improved patient survival rates(2, 3). However, these treatments are effective only for patients with specific genetic mutations (e.g., epidermal growth factor receptor and anaplastic lymphoma kinase) or high PD-L1 expression, which limits the eligible patient population, and the development of drug resistance after treatment remains a major challenge(4, 5). Therefore, there is an urgent need to identify new therapeutic targets and develop effective treatment strategies for LUAD.

The tripartite motif (TRIM) family of proteins consists of E3 ubiquitin ligases involved in various biological processes that play crucial roles in cell growth, differentiation, immune responses, and tumorigenesis(6). *TRIM29* is a TRIM protein that influences the stability and function of various target proteins through ubiquitination (7). TRIM29 overexpression has been repeatedly associated with adverse outcomes and pro-tumorigenic signaling, such as epithelial–mesenchymal transition (EMT)(8), proliferation(9) and enhanced invasion(10) in several tumor types. A previous study revealed that TRIM29 levels positively correlate with tumor size, adverse histologic grade, advanced TNM staging, and lymphatic nodal metastasis in LUAD(11).

However, the functional role of *TRIM29* and its impact on the tumor microenvironment (TME) in LUAD have not yet been elucidated. Therefore, this study aimed to elucidate the role of *TRIM29* in LUAD using four independent LUAD datasets to perform gene set enrichment analysis (GSEA) and tumor microenvironment deconvolution. Through this, we identified the role of *TRIM29* in the TME and validated our findings through histopathological and immunohistochemical analyses, as well as cell line studies. Furthermore, we conducted a drug sensitivity analysis to identify candidate agents that effectively inhibit *TRIM29*. This study proposes *TRIM29* as a new therapeutic target for LUAD and contributes to the development of new treatment strategies.

Materials and methods

Study population

We investigated four LUAD cohorts: the Pan-Cancer Atlas RNA-seq (n = 510) and CPTAC-LUAD (n = 110) cohorts obtained from cBioPortal (http://cbioportal.org)(12), a resected LUAD series from Ajou University Hospital (n = 200), and the KM plotter LUAD compendium (n = 1,161; https://kmplot.com)(13). The demographic and clinicopathological features of the Ajou cohort are summarized in Supplementary Table 1. The study protocol was approved by the Institutional Review Board of Ajou University Hospital (IRB No. AJOUIRB-KS-2024-340, approved on July 11, 2024), and the requirement for informed consent was waived by the same Institutional Review Board due to the retrospective nature of the study. All procedures complied with the principles of the Declaration of Helsinki. Identifiers were removed from all images.

Histopathology and immunohistochemistry

Tissue microarrays were generated and stained for *TRIM29*, E-cadherin, SNAI1 (SNAIL), TWIST1 (TWIST), VIMENTIN, and CD31. Antibody information is provided in Supplementary Table 2. Staining was performed on the VENTANA BenchMark ULTRA platform using the OptiView DAB detection system. Cytoplasmic or membranous staining intensity in tumor cells was graded 0–3, and expression was summarized using an H-score (intensity × percentage of positive cells)(14). For microvessel density (MVD), CD31 highlighted vascular structures and angiogenic “hotspots

were identified at low power (×40), and microvessels were counted in three random high-power fields (×400) per case, with the mean recorded as the MVD. Stromal proportion was evaluated as previously described(15), where the largest invasive block was located at 1.25×, and at 10×, only fields containing both stroma and tumor were scored, estimating the stromal area in 5% increments.

Cell culture

Human LUAD lines (NCI-H441 and NCI-H650; Korean Cell Line Bank) were maintained in RPMI-1640 supplemented with 10% fetal bovine serum and 1% penicillin–streptomycin at 37 °C in 5% CO_2. All cell lines were tested negative for mycoplasma before the experiments.

TRIM29 siRNA transfection

Small interfering RNAs (siRNAs) were transfected using Lipofectamine RNAiMAX (Invitrogen) according to the manufacturer's instructions. siRNA #1: sense, 5′-CCAAUGAGAAGGCCAUCCU-3′; antisense, 5′-AGGAUGGCCUUCUCAUUGG-3′. siRNA #2: sense, 5′-CCACCUAUCAUGUCCUGCU-3′; antisense, 5′-AGCAGGACAUGAUAGGUGG-3′.

Western blotting

The cells were lysed using RIPA buffer (Thermo Fisher Scientific). Proteins were separated using sodium dodecyl sulfate-polyacrylamide gel electrophoresis, transferred to polyvinylidene difluoride membranes, and probed with antibodies against *TRIM29*, E-cadherin, N-cadherin, SNAIL, and TWIST (Supplementary Table 2).

Cell Migration Analysis

Cell migration was evaluated via a wound healing assay performed on confluent monolayers 24h post-transfection. A sterile tip was used to create a linear scratch, followed by a PBS wash and incubation in 1% FBS medium to isolate migration from proliferation. The healing process was monitored microscopically over a 96-hour period. Wound areas were analyzed using ImageJ, and the percentage of closure was calculated by comparing the wound area at each time point (24, 48, 72, 96 hour) against the initial area at 0h. The change in scratch-wound area was calculated using the following equation:

Wound Closure (%) = [(scratch-wound area at 0 h - scratch-wound area at 24, 48, 72, 96 hour) / (scratch-wound area at 0 h)] × 100 (%)

GSEA

GSEA (v4.3.2; Broad Institute; http://www.broadinstitute.org/gsea/index.jsp)(16) was performed using the hallmark gene sets. Samples were dichotomized according to median

TRIM29 expression. Nominal p-values were estimated from 1,000 phenotype permutations in this study.

Tumor microenvironment analysis using deconvolution tools (xCell, ESTIMATE, EPIC)

Signals from non-malignant cell populations were inferred from bulk expression using three complementary tools. xCells produced enrichment scores for 64 immune/stromal cell types and composite immune, stromal, and microenvironment scores(17). ESTIMATE yields an immune score, stromal score, and combined ESTIMATE Score(18). EPIC was used to estimate the cell type proportions from the bulk profiles(19).

Construction of TRIM29-associated Transcriptional Module

To transition from a single-gene centric analysis to a system-level approach, a *TRIM29*-associated transcriptional module was constructed. First, Spearman's rank correlation coefficients (rho) were calculated between the expression of *TRIM29* and all other protein-coding genes across the entire transcriptome. Genes within the top 5th percentile of the highest positive correlation were selected to define the *TRIM29*-coexpression module. To represent the collective activity of this module, a composite module score was calculated for each sample by averaging the Z-score transformed expression values of the constituent genes. Samples were then stratified into "Module-High" and "Module-Low" groups based on the median score for subsequent downstream analyses, including TME

deconvolution and functional enrichment.

Drug Sensitivity analysis

We analyzed the LUAD cell lines from the DepMap database. To measure drug sensitivity, we used the PRISM repurposing secondary screening dataset (PRISM, Profiling Relative Inhibition Simultaneously in Mixtures; AUC) and the Genomics of Drug Sensitivity in Cancer datasets (GDSC1/2; IC50 and AUC), where AUC is the area under the dose–response viability curve and IC50 is the half-maximal inhibitory concentration. The cell lines were split into *TRIM29*-HIGH and -LOW by the top/bottom 20% (with tertile or median split fallback when the groups were small). For drugs with ≥8 LUAD lines, we tested association using Spearman correlation—where a negative Spearman ρ indicates that higher *TRIM29* expression is associated with lower AUC/IC50 values (greater drug sensitivity)—and a two-sided Wilcoxon rank-sum test comparing HIGH vs. LOW; *p* values were false discovery rate (FDR)-adjusted (Benjamini–Hochberg). PRISM and GDSC results were integrated per compound using Fisher's method on Spearman *p* values, together with the minimum FDR and mean ρ; only direction-concordant hits were ranked, and the top 50 negative associations were reported. For visualization, the AUC was z-scored within each drug for heatmaps. All analyses were performed using R software (tidyverse, limma, and pheatmap packages).

Statistical analysis

Between-group differences in continuous variables were tested using the Mann–Whitney U test. Correlations were calculated using Spearman's rank test. Survival was analyzed using Kaplan–Meier estimates and log-rank tests. Deconvolution analyses were performed in R with xCell, ESTIMATE, and EPIC. The TRIM29 cutoff point for survival in the Ajou cohort was selected using Cutoff Finder based on the log-rank significance(20). Statistical analyses were conducted using IBM SPSS Statistics (version 25.0; IBM, Armonk, NY, USA) and R 4.3.3 (http://www.r-project.org/). Statistical significance was defined as two-sided $p < 0.05$.

Results

GSEA-based analysis of signaling pathways associated with *TRIM29* expression in LUAD

To explore the signaling pathways associated with *TRIM29* expression, we conducted GSEA using the median *TRIM29* expression level as the threshold for group stratification. Figure 1 presents the ten pathways with the highest normalized enrichment scores (NES) identified in the two independent mRNA expression datasets. Among these, the apical junction, EMT, and KRAS signaling UP consistently emerged as enriched in the *TRIM29*-high cohort. In the Pan-Cancer Atlas dataset, tumors with elevated *TRIM29* expression were significantly enriched in the EMT pathway (NES = 1.78, $p = 0.018$, FDR = 0.048; Figure 1A, B). A similar pattern was observed in the CPTAC dataset, in which EMT enrichment was

detected in the *TRIM29*-high group (NES = 1.56, $p = 0.083$, FDR = 0.235; Figure 1C, D).

Deconvolution-based characterization of the tumor microenvironment in relation to *TRIM29* expression in LUAD

We next examined the association between *TRIM29* expression and the TME in two independent LUAD cohorts (The Cancer Genome Atlas (TCGA) and the Clinical Proteomic Tumor Analysis Consortium (CPTAC)). In the TCGA dataset, xCell deconvolution revealed that *TRIM29*-high tumors were characterized by increased enrichment of fibroblasts and endothelial cells, and higher stromal and microenvironment scores than *TRIM29*-low tumors (*all* $p < 0.05$; Figure 2A). Concordant results were obtained using ESTIMATE, which showed significantly elevated ESTIMATE, immune, and stromal scores in the *TRIM29*-high group (*all* $p < 0.05$; Figure 2B). Similarly, EPIC analysis confirmed a greater proportion of cancer-associated fibroblasts ($p = 0.02$; Figure 2C) and suggested a trend toward increased endothelial cell content, although this was not statistically significant ($p = 0.08$; Figure 2C).

The enrichment patterns were consistent in the CPTAC LUAD cohort. *TRIM29*-high tumors exhibited higher levels of fibroblasts ($p = 0.02$; Figure 3A), endothelial cells ($p = 0.002$; Figure 3A), and stromal/microenvironment scores ($p = 0.04$, $p = 0.09$, respectively;

Figure 3A) than xCell analysis. ESTIMATE analysis further supported these findings, with significantly higher ESTIMATE, immune, and stromal scores in the *TRIM29*-high group (*all* $p < 0.001$; Figure 3B). The EPIC analysis revealed a strong association between *TRIM29* expression and endothelial cell enrichment ($p = 0.004$; Figure 3C), whereas cancer-associated fibroblasts showed no significant correlation ($p = 0.61$; Figure 3C).

Overall, these findings indicate that elevated *TRIM29* expression is consistently linked to stromal activation in LUAD, as reflected by endothelial cell enrichment and fibroblast infiltration.

Characterization of the tumor microenvironment in relation to the *TRIM29*-associated transcriptional module

To shift from a single-gene-centric view to a network-level perspective, we defined a *TRIM29*-associated transcriptional module comprising the top 5% of genes most strongly correlated with *TRIM29* expression. We then characterized the TME landscape by stratifying patients into module-high and module-low groups across two independent LUAD cohorts.

To explore the signaling pathways coordinated by the *TRIM29*-associated transcriptional module, we conducted GSEA using the median module score as the threshold for group stratification. Figure 4 illustrates the top ten hallmark pathways with the highest NES in both

cohorts. In the TCGA dataset, the EMT pathway exhibited the strong association with the module activity, characterized by high enrichment scores and significant statistical stringency (NES = 2.26, $p < 0.001$, FDR < 0.001; Figure 4A, B). This pattern was remarkably consistent in the CPTAC dataset. The *TRIM29*-associated module was again top-ranked for the EMT pathway, showing even higher enrichment magnitude than the single-gene analysis (NES = 2.31, $p < 0.001$, FDR < 0.001; Figure 4C, D).

In the TCGA dataset, xCell deconvolution demonstrated that module-high tumors were significantly enriched with fibroblasts and endothelial cells, exhibiting markedly higher stromal and microenvironment scores compared to module-low tumors (all $p < 0.001$; Supplementary Figure 1A). These findings were further corroborated by ESTIMATE analysis, which revealed significantly elevated stromal, immune, and overall ESTIMATE scores in the module-high group (all $p < 0.001$; Supplementary Figure 1B). Additionally, EPIC analysis confirmed a substantially higher fraction of cancer-associated fibroblasts ($p < 0.001$) and endothelial cells ($p = 0.031$) in tumors with high module activity (Supplementary Figure 1C). The association between the *TRIM29* module and stromal activation was consistently observed in the CPTAC LUAD cohort. According to xCell analysis, module-high tumors showed significantly increased infiltration of fibroblasts ($p < 0.001$; Supplementary Figure 2A) and endothelial cells ($p = 0.002$; Supplementary Figure 2A), alongside higher stromal ($p < 0.001$;

Supplementary Figure 2A) and microenvironment scores (p = 0.008; Supplementary Figure 2A). ESTIMATE scores supported this trend, with significantly higher stromal (p = 0.016; Supplementary Figure 2B) and ESTIMATE scores (p = 0.039; Supplementary Figure 2B) in the module-high group, although the difference in immune scores did not reach statistical significance (p = 0.174; Supplementary Figure 2B). EPIC analysis further validated the enrichment of endothelial cells in the module-high group (p = 0.001; Supplementary Figure 2C). However, in contrast to the endothelial enrichment, cancer-associated fibroblasts fractions were found to be significantly higher in the module-low group (p = 0.025; Supplementary Figure 2C).

Immunohistochemical and histopathological validation of *TRIM29*-associated biological processes

To validate the association between TRIM29 expression and tumor biology, we performed immunohistochemical and histopathological analyses of 200 LUAD specimens obtained from Ajou University Hospital. Representative staining images of TRIM29, EMT markers (E-cadherin and vimentin), EMT-inducing transcription factors (EMT-TFs) (SNAIL and TWIST), MVD, and stromal proportions are shown in Figure 5A.

Correlation analysis demonstrated that TRIM29 expression was not significantly correlated with that of E-cadherin (*Rho* = -0.017, p = 0.806;

Figure 5B) or VIMENTIN (*Rho* = 0.045, $p = 0.533$; Figure 5C). In contrast, TRIM29 expression in tumor cells was positively associated with SNAIL and TWIST expression (*Rho* = 0.192, $p = 0.007$; *Rho* = 0.243, $p < 0.001$; Figure 5D and E), MVD (*Rho* = 0.201, $p < 0.001$; Figure 5F), and stromal proportion (*Rho* = 0.154, $p = 0.033$; Figure 5G). Collectively, these findings support the association between TRIM29 expression and the upregulation of EMT-inducing transcription factors (EMT-TFs), such as SNAIL and TWIST, as well as angiogenesis and stromal remodeling in LUAD, although a direct correlation with canonical phenotypic EMT markers was not observed.

Prognostic implications of *TRIM29* expression

Next, we investigated the prognostic significance of *TRIM29* expression in patients with LUAD. Using the KM plotter LUAD dataset (n = 1,161), Kaplan–Meier analysis revealed that patients with higher *TRIM29* mRNA expression had significantly shorter overall survival ($p = 0.00073$; Figure 6A). Similarly, analysis of the Ajou University Hospital LUAD cohort (n = 200), in which TRIM29 protein expression was dichotomized at an H-score threshold of 100, demonstrated that elevated TRIM29 protein levels were strongly associated with poor survival outcomes ($p < 0.001$; Figure 6B). Multivariate Cox regression analysis further confirmed that TRIM29 expression was an independent prognostic marker of LUAD (hazard ratio = 3.061, $p = 0.048$; Figure 6C).

Role of *TRIM29* in EMT pathway and *TRIM29*–Drug Sensitivity in

DepMap LUAD

To determine whether *TRIM29* is functionally involved in the EMT pathway in LUAD cells, we conducted a series of in vitro experiments. In two LUAD cell lines, TRIM29 suppression significantly decreased the expression of EMT-inducing transcription factors (EMT-TFs), such as SNAIL and TWIST (Figure 7A). Furthermore, we observed a classic 'cadherin switch' characterized by an increase in E-cadherin and a decrease in N-cadherin levels following TRIM29 inhibition (Figure 7A). To evaluate the functional consequences of these molecular changes, we performed a wound healing assay, which revealed that TRIM29 knockdown markedly reduced the migratory capacity of LUAD cells (Figure 7B). Collectively, these findings provide robust evidence that TRIM29 drives the EMT program and promotes cellular migration in LUAD.

We prioritized the top 50 compounds from the PRISM Repurposing Secondary Screen (AUC) and GDSC1/2 (IC50/AUC), which showed a negative association between *TRIM29* expression and drug response (i.e., higher *TRIM29* expression correlated with a lower AUC/IC50, indicating greater sensitivity). These compounds were identified as candidate agents with preferential activity in the *TRIM29*-high context. For the PRISM subset (46 compounds with sufficient coverage), the compound–cell line relationships were visualized as a heatmap (Figure 7C). Across all drugs, the *TRIM29*-HIGH group consistently exhibited lower AUC

values than the LOW group, consistent with increased sensitivity. Next, we summarized the mechanisms of action of the top 50 and observed the enrichment of mTOR inhibitors (n = 5: compound names PF-05212384, OSI-027, torin-2, torin-1, and PP242) (Figure 7D).

Discussion

To the best of our knowledge, this is the first study to provide evidence that *TRIM29* is significantly associated with EMT-inducing transcriptional program, angiogenesis, and stromal remodeling in LUAD, emphasizing the novelty and clinical relevance of our findings. Consistent associations were detected in two independent LUAD transcriptomic datasets and subsequently confirmed at the protein level in an independent cohort of patients. High *TRIM29* expression was associated with poor clinical outcomes. Moreover, TRIM29 expression was associated with EMT-related phenotypes in cell line models, and drug response analyses suggested mTOR inhibitors as potential treatment options for *TRIM29*-high tumors.

Our drug response analyses identified mTOR inhibitors as the primary candidate therapies for tumors exhibiting high *TRIM29* expression. This finding is supported by recent studies that have highlighted a critical functional link between *TRIM29* and the mTOR signaling pathway. Elevated, elevated *TRIM29* expression acts as an oncogene in nasopharyngeal carcinoma. Mechanistically, it reduced the levels of the tumor suppressor PTEN and increased the phosphorylation of AKT, p70S6K, and 4E-BP1 in the cells. The pro-invasive effects of *TRIM29* were

functionally reversed by AKT inhibition or treatment with rapamycin, a well-known mTOR inhibitor, thus establishing a direct connection between *TRIM29*-driven invasiveness and the *PTEN/AKT/*mTOR signaling pathway(21). A recent study indicated that *TRIM29* enhances cell proliferation and metastasis in colorectal cancer through indirect modulation of the *PI3K/AKT* pathway(22). *TRIM29* drives thyroid carcinoma progression by activating the *PI3K/AKT* signaling pathway(23). However, our GSEA results for the *PI3K/AKT/*mTOR pathway in the Pancancer and CPTAC datasets did not reach statistical significance at the mRNA level. Therefore, the mTOR inhibitor signal likely reflects an indirect, context-dependent suppression of *TRIM29*-associated downstream programs, rather than direct inhibition of *TRIM29* itself. *AKT/*mTOR signaling has been closely linked to EMT regulation. A comprehensive review by Roshan et al. summarizes multiple mechanisms by which *AKT/*mTOR activation promotes EMT, including induction of EMT transcription factors (e.g., SNAIL, ZEB, and TWIST) and suppression of epithelial traits such as E-cadherin expression(24). Consistent with this, Perumal et al. showed in lung cancer cells that *PTEN* inactivation, an upstream event that enhances *PI3K–AKT–*mTOR signaling, can drive EMT-associated programs through *β-catenin/SNAIL*-related pathways(25). Collectively, these studies support the biological plausibility that mTOR-axis activity can contribute to EMT-like states. Accordingly, even without transcript-level pathway enrichment in our cohorts, mTOR inhibitors may still indirectly attenuate the *TRIM29*–EMT program by suppressing EMT-

promoting signaling.

Previous studies have implicated *TRIM29* in the regulation of EMT, angiogenesis, and stromal remodeling. In lung squamous cell carcinoma, *TRIM29* promotes cell proliferation, migration, and invasion by driving the autophagic degradation of E-cadherin and altering EMT markers(26). In nasopharyngeal carcinoma, ectopic *TRIM29* expression enhances cell proliferation, EMT, and invasion(21). *TRIM29* is transcriptionally upregulated under hypoxia via *ATM/HIF-1α*, positioning it within the canonical pro-angiogenic stress program(27). In lung cancer cells, *TRIM29* upregulates *MMP-9* through ERK/JNK, a protease central to extracellular matrix (ECM) degradation, invasion, and angiogenesis, thereby providing a direct conduit from *TRIM29* to matrix remodeling(28). Beyond controlling proteases, *TRIM29* rewires adhesion and cytoskeletal circuitry by inducing autophagic E-cadherin turnover in lung cancer and modulating intermediate filaments and focal adhesions in bladder cancer, changes integral to tumor–stroma communication and ECM dynamics (26, 28).

We used three complementary bulk transcriptome deconvolution tools, xCell, ESTIMATE, and EPIC, to characterize the relationship between *TRIM29* and the LUAD tumor microenvironment. xCell is a gene-signature-based framework that infers the enrichment of 64 immune and stromal cell types and provides composite microenvironment/stromal metrics, enabling broad cell-state-aware profiling from bulk data(17). ESTIMATE computes stromal, immune, and aggregate ESTIMATE scores via single-

sample gene set enrichment analysis-derived signatures, and has been shown to correlate with tumor purity, thereby offering an orthogonal view of non-malignant admixture in tumors (18). EPIC deconvolves the proportions of major immune and non-immune stromal compartments (including cancer-associated fibroblasts and endothelial cells) using RNA-seq reference profiles and renormalization to account for cell-type-specific mRNA content, providing proportion-level readouts that complement the enrichment score (19). Applying these methods across two independent LUAD cohorts, we observed concordant increases in fibroblast and endothelial signals, as well as higher stromal/microenvironment and ESTIMATE scores in *TRIM29*-high tumors, supporting a robust association between *TRIM29* expression and stromal activation. Although each method has intrinsic limitations, cross-tool agreement mitigates method-specific biases and strengthens the inferences. These results, together with our immunohistochemical findings, suggest that *TRIM29*-high LUADs reside in a stroma-rich, vascularized milieu that is likely to influence invasion, immune exclusion, and therapeutic responses, motivating orthogonal validation with spatial or single-cell assays in future studies.

Histopathologically, a high stromal rate reflects a desmoplastic, fibroblast-rich, and ECM-rich microenvironment. In NSCLC, stroma-poor cases show better outcomes than stroma-rich tumors, supporting the clinical relevance of a high stromal rate in thoracic oncology(29-31). Mechanistically, stromal activation coordinates CAF-driven immune exclusion(32), ECM remodeling/stiffening(33), and proangiogenic

signaling(34), which facilitates EMT, invasion, and resistance to therapy. Transcriptomic analyses revealed that *TRIM29*-high tumors exhibited significantly higher stromal and microenvironment scores, and patients in the *TRIM29*-high group had a poorer prognosis. This integrated pathology–transcriptome–outcome framework strengthens the rationale for biomarker-enriched therapeutic strategies for *TRIM29*-high tumors.

In the Ajou validation cohort, *TRIM29* expression showed a significant positive correlation with EMT-inducing transcription factors (EMT-TFs), specifically *SNAIL* and *TWIST*, even though canonical phenotypic markers did not reach significance. This suggests that in the complex tumor microenvironment of LUAD, *TRIM29* may primarily function as an upstream initiator of the EMT transcriptional program. It is well-established that the TGF-β and Wnt/β-catenin axes play pivotal roles in the transcriptional regulation of EMT(35, 36). The lack of correlation with E-cadherin/vimentin in tissue might be due to the transient nature of EMT or the presence of a "partial EMT" state, which is frequently observed in clinical carcinoma samples(37, 38).

Our study had certain limitations. First, although combined mRNA/immunohistochemical data and cell line assays support a relationship between *TRIM29* and EMT, angiogenesis, and prognosis, the pathway-level mediators of these effects were not evaluated in this study. Definitive causal inference requires focused mechanistic experiments using cellular and animal models. Second, protein quantification relies on tissue microarrays, which are susceptible to sampling bias due to

pronounced intratumoral heterogeneity. Third, our transcriptomic and protein datasets were not perfectly matched at the specimen level, and this lack of concordant sampling may have contributed to the variability in cross-modal comparisons. Fourth, our inference of tumor microenvironment composition was based on computational deconvolution methods (xCell, ESTIMATE, and EPIC), which rely on predefined gene signatures and may not fully capture the complexity and spatial heterogeneity of the tumor microenvironment. Direct validation using spatially resolved or single-cell approaches would strengthen these findings. Fifth, the retrospective design and heterogeneity across cohorts, including differences in clinical characteristics, treatment regimens, and sequencing platforms, may have introduced confounding factors that could influence survival and gene expression analyses.

This is the first study to systematically implicate *TRIM29* in LUAD progression through the coordinated promotion of EMT-related transcriptional program, angiogenesis, and stromal remodeling. By transitioning from a single-gene focus to the definition of a *TRIM29*-associated transcriptional module, we demonstrate that *TRIM29* does not function in isolation but rather orchestrates a robust co-expression network that drives these hallmark biological processes. These module-level signatures were concordant across two independent transcriptomic cohorts and were corroborated at the protein level in a separate LUAD cohort, underscoring the robustness of our findings. High *TRIM29* expression is associated with an adverse prognosis. Consistent with these

observations, *TRIM29* was associated with EMT-related phenotypes in cell line models, and pharmacogenomic analyses suggested mTOR inhibitors as potential candidates for *TRIM29*-high tumors. Collectively, the data position *TRIM29* as both a prognostic biomarker and a promising therapeutic target in LUAD and motivate future studies to elucidate the mechanisms of *TRIM29*-driven stromal activation and test strategies that disrupt *TRIM29*-mediated tumor–stroma interactions.

Data availability

The datasets generated during and/or analysed during the current study are available from the corresponding author on reasonable request.

Acknowledgements

None

Author contributions

Conception and design: Young Wha Koh, Financial support: Young Wha Koh, Collection and assembly of data: Yoonjung Hwang, Jae-Ho Han, Seokjin Haam and Hyun Woo Lee, Data analysis and interpretation: Young Wha Koh and Yoonjung Hwang, Manuscript writing: All authors, Final approval of manuscript: All authors, Accountable for all aspects of

the work: All authors

Funding

This research was supported by the Basic Science Research Program through the National Research Foundation of Korea (NRF) funded by the Ministry of Science, ICT (RS-2024-00336500 for Young Wha Koh).

Declarations

Competing interests

The authors declare no competing interests.

Reference

1. Siegel RL, Giaquinto AN, Jemal A. Cancer statistics, 2024. CA Cancer J Clin. 2024;74(1):12-49.
2. Borghaei H, Paz-Ares L, Horn L, Spigel DR, Steins M, Ready NE, et al. Nivolumab versus Docetaxel in Advanced Nonsquamous Non-Small-Cell Lung Cancer. N Engl J Med. 2015;373(17):1627-39.
3. Soria JC, Ohe Y, Vansteenkiste J, Reungwetwattana T, Chewaskulyong B, Lee KH, et al. Osimertinib in Untreated EGFR-Mutated Advanced Non-Small-Cell Lung Cancer. N Engl J Med. 2018;378(2):113-25.
4. Morgillo F, Della Corte CM, Fasano M, Ciardiello F. Mechanisms of resistance to EGFR-targeted drugs: lung cancer. ESMO Open. 2016;1(3):e000060.
5. Sharma P, Hu-Lieskovan S, Wargo JA, Ribas A. Primary, Adaptive, and Acquired Resistance to Cancer Immunotherapy. Cell. 2017;168(4):707-23.
6. Nisole S, Stoye JP, Saïb A. TRIM family proteins: retroviral restriction and antiviral defence. Nat Rev Microbiol. 2005;3(10):799-808.
7. Lv K, Li Q, Jiang N, Chen Q. Role of TRIM29 in disease: What is and is not known. International Immunopharmacology. 2025;147:113983.
8. Sun J, Zhang T, Cheng M, Hong L, Zhang C, Xie M, et al. TRIM29 facilitates the epithelial-to-mesenchymal transition and the progression of colorectal cancer via the activation of the Wnt/β-catenin signaling pathway. J Exp Clin Cancer Res. 2019;38(1):104.
9. Tan S-T, Liu S-Y, Wu B. TRIM29 Overexpression Promotes Proliferation and Survival of Bladder Cancer Cells through NF-κB Signaling. Cancer Res Treat. 2016;48(4):1302-12.
10. Wang L, Yang H, Abel EV, Ney GM, Palmbos PL, Bednar F, et al. ATDC induces an invasive switch in KRAS-induced pancreatic tumorigenesis. Genes & Development. 2015;29(2):171-83.
11. Zhou Z-Y, Yang G-Y, Zhou J, Yu M-H. Significance of TRIM29 and β-catenin

expression in non-small-cell lung cancer. Journal of the Chinese Medical Association. 2012;75(6):269-74.
12. Cerami E, Gao J, Dogrusoz U, Gross BE, Sumer SO, Aksoy BA, et al. The cBio cancer genomics portal: an open platform for exploring multidimensional cancer genomics data. Cancer discovery. 2012;2(5):401-4.
13. Győrffy B. Transcriptome-level discovery of survival-associated biomarkers and therapy targets in non-small-cell lung cancer. Br J Pharmacol. 2023.
14. McCarty KS, Jr., Szabo E, Flowers JL, Cox EB, Leight GS, Miller L, et al. Use of a monoclonal anti-estrogen receptor antibody in the immunohistochemical evaluation of human tumors. Cancer research. 1986;46(8 Suppl):4244s-8s.
15. Mesker WE, Junggeburt JM, Szuhai K, de Heer P, Morreau H, Tanke HJ, et al. The carcinoma–stromal ratio of colon carcinoma is an independent factor for survival compared to lymph node status and tumor stage. Analytical Cellular Pathology. 2007;29(5):387-98.
16. Subramanian A, Tamayo P, Mootha VK, Mukherjee S, Ebert BL, Gillette MA, et al. Gene set enrichment analysis: a knowledge-based approach for interpreting genome-wide expression profiles. Proceedings of the National Academy of Sciences. 2005;102(43):15545-50.
17. Aran D, Hu Z, Butte AJ. xCell: digitally portraying the tissue cellular heterogeneity landscape. Genome Biol. 2017;18(1):220.
18. Yoshihara K, Shahmoradgoli M, Martínez E, Vegesna R, Kim H, Torres-Garcia W, et al. Inferring tumour purity and stromal and immune cell admixture from expression data. Nat Commun. 2013;4:2612.
19. Racle J, Gfeller D. EPIC: A Tool to Estimate the Proportions of Different Cell Types from Bulk Gene Expression Data. Methods Mol Biol. 2020;2120:233-48.
20. Budczies J, Klauschen F, Sinn BV, Győrffy B, Schmitt WD, Darb-Esfahani S, et al. Cutoff Finder: a comprehensive and straightforward Web application enabling rapid biomarker cutoff optimization. PLoS One. 2012;7(12):e51862.
21. Zhou XM, Sun R, Luo DH, Sun J, Zhang MY, Wang MH, et al. Upregulated TRIM29 promotes proliferation and metastasis of nasopharyngeal carcinoma via PTEN/AKT/mTOR signal pathway. Oncotarget. 2016;7(12):13634-50.
22. Jiang T, Wang H, Liu L, Song H, Zhang Y, Wang J, et al. CircIL4R activates the PI3K/AKT signaling pathway via the miR-761/TRIM29/PHLPP1 axis and promotes proliferation and metastasis in colorectal cancer. Mol Cancer. 2021;20(1):167.
23. Xu J, Li Z, Su Q, Zhao J, Ma J. TRIM29 promotes progression of thyroid carcinoma via activating P13K/AKT signaling pathway. Oncol Rep. 2017;37(3):1555-64.
24. Karimi Roshan M, Soltani A, Soleimani A, Rezaie Kahkhaie K, Afshari AR, Soukhtanloo M. Role of AKT and mTOR signaling pathways in the induction of epithelial-mesenchymal transition (EMT) process. Biochimie. 2019;165:229-34.
25. Perumal E, So Youn K, Sun S, Seung-Hyun J, Suji M, Jieying L, et al. PTEN inactivation induces epithelial-mesenchymal transition and metastasis by intranuclear translocation of β-catenin and snail/slug in non-small cell lung carcinoma cells. Lung Cancer. 2019;130:25-34.
26. Xu W, Chen B, Ke D, Chen X. TRIM29 mediates lung squamous cell carcinoma cell metastasis by regulating autophagic degradation of E-cadherin. Aging (Albany NY). 2020;12(13):13488-501.
27. Dükel M, Streitfeld WS, Tang TC, Backman LR, Ai L, May WS, et al. The Breast Cancer Tumor Suppressor TRIM29 Is Expressed via ATM-dependent Signaling in Response to Hypoxia. J Biol Chem. 2016;291(41):21541-52.
28. Tang ZP, Cui QZ, Dong QZ, Xu K, Wang EH. Ataxia-telangiectasia group D complementing gene (ATDC) upregulates matrix metalloproteinase 9 (MMP-9) to promote lung cancer cell invasion by activating ERK and JNK pathways. Tumour Biol. 2013;34(5):2835-42.
29. Xi K-X, Wen Y-S, Zhu C-M, Yu X-Y, Qin R-Q, Zhang X-W, et al. Tumor-stroma ratio (TSR) in non-small cell lung cancer (NSCLC) patients after lung resection is a prognostic factor for survival. Journal of Thoracic Disease. 2017;9(10):4017-26.
30. Zhang T, Xu J, Shen H, Dong W, Ni Y, Du J. Tumor-stroma ratio is an independent predictor for survival in NSCLC. Int J Clin Exp Pathol. 2015;8(9):11348-55.

31. Smit MA, Philipsen MWH, Postmus PE, Putter H, Tollenaar RAEM, Cohen D, et al. The prognostic value of the tumor-stroma ratio in squamous cell lung cancer, a cohort study. Cancer Treatment and Research Communications. 2020;25:100247.
32. Monteran L, Erez N. The Dark Side of Fibroblasts: Cancer-Associated Fibroblasts as Mediators of Immunosuppression in the Tumor Microenvironment. Front Immunol. 2019;10:1835.
33. Jiang Y, Zhang H, Wang J, Liu Y, Luo T, Hua H. Targeting extracellular matrix stiffness and mechanotransducers to improve cancer therapy. Journal of Hematology & Oncology. 2022;15(1):34.
34. Bordeleau F, Mason BN, Lollis EM, Mazzola M, Zanotelli MR, Somasegar S, et al. Matrix stiffening promotes a tumor vasculature phenotype. Proc Natl Acad Sci U S A. 2017;114(3):492-7.
35. Xu J, Lamouille S, Derynck R. TGF-beta-induced epithelial to mesenchymal transition. Cell Res. 2009;19(2):156-72.
36. Xue W, Yang L, Chen C, Ashrafizadeh M, Tian Y, Sun R. Wnt/β-catenin-driven EMT regulation in human cancers. Cell Mol Life Sci. 2024;81(1):79.
37. Pastushenko I, Blanpain C. EMT Transition States during Tumor Progression and Metastasis. Trends in Cell Biology. 2019;29(3):212-26.
38. Karacosta LG, Anchang B, Ignatiadis N, Kimmey SC, Benson JA, Shrager JB, et al. Mapping lung cancer epithelial-mesenchymal transition states and trajectories with single-cell resolution. Nature Communications. 2019;10(1):5587.

Figure Legends

Figure 1. GSEA stratified by *TRIM29* expression in the two LUAD cohorts. Top 10 pathways enriched in *TRIM29*-high tumors in the Pan-Cancer Atlas (A) and CPTAC (C). Enrichment plots for EMT by *TRIM29* expression in

the Pan-Cancer Atlas (B) and CPTAC (D).

Abbreviations: EMT, epithelial–mesenchymal transition; GSEA, gene set enrichment analysis; LUAD, lung adenocarcinoma; NES, normalized enrichment score

Figure 2. Association of *TRIM29* with stromal/immune features in the TCGA-LUAD cohort. xCell-inferred stromal and endothelial populations (A); ESTIMATE immune/stromal scores (B); EPIC-inferred fractions of cancer-associated fibroblasts and endothelial cells (C).

Abbreviations: LUAD, lung adenocarcinoma; CAF, cancer-associated fibroblast

Figure 3. Association of *TRIM29* with stromal/immune features in the CPTAC-LUAD cohort. xCell-inferred stromal and endothelial populations (A); ESTIMATE scores (B); EPIC-inferred fractions of CAFs and endothelial cells (C).

Abbreviations: LUAD, lung adenocarcinoma; CAF, cancer-associated fibroblast

Figure 4. GSEA stratified by *TRIM29*-associated transcriptional module in the two LUAD cohorts. Top 10 pathways enriched in *TRIM29*-associated transcriptional module -high tumors in the Pan-Cancer Atlas (A) and CPTAC (C). Enrichment plots for EMT by *TRIM29*-associated transcriptional module in the Pan-Cancer Atlas (B) and CPTAC (D).

Abbreviations: EMT, epithelial–mesenchymal transition; GSEA, gene set enrichment analysis; LUAD, lung adenocarcinoma; NES, normalized enrichment score

Figure 5. Correlations between TRIM29 and EMT, angiogenesis, and stromal content in LUAD specimens from Ajou University Hospital. Representative IHC images of TRIM29 (magnification x400 and scale bar is 50um), EMT markers (magnification x400 and scale bar is 50um), microvessel density (MVD) (magnification x400 and scale bar is 50um), and stromal proportion (magnification x100 and scale bar is 200um) (A). Correlations of TRIM29 with E-cadherin (B), vimentin (C), SNAIL (D), TWIST (E), MVD (F), and stromal proportion (G)

Abbreviations: EMT, epithelial–mesenchymal transition; LUAD, lung adenocarcinoma; MVD, microvessel density; IHC, immunohistochemistry

Figure 6. Survival according to *TRIM29* expression in the KM plotter and Ajou University Hospital LUAD datasets. Overall survival by *TRIM29* level in the KM plotter (A) and Ajou cohort (B). Multivariable analysis of overall survival in the Ajou cohort (C).

Abbreviations: LUAD, lung adenocarcinoma

Figure 7. *TRIM29* function in the EMT pathway and TRIM29–drug sensitivity in DepMap LUAD. TRIM29 knockdown versus control in NCI-H441 and NCI-H650 cells (A). Wound healing assay according to TRIM29

knockdown in NCI-H441 and NCI-H650 cells (B). Heatmap of compound–cell line responses in the PRISM dataset (C). Bar chart showing the mechanism-of-action frequency among the top 50 compounds (D).

Abbreviations: EMT, epithelial–mesenchymal transition; DepMap, Cancer Dependency Map; PRISM, Profiling Relative Inhibition Simultaneously in Mixtures; MOA, mechanism of action

Supplementary Figure 1. Association of *TRIM29*-associated transcriptional module with stromal/immune features in the TCGA-LUAD cohort. xCell-inferred stromal and endothelial populations (A); ESTIMATE immune/stromal scores (B); EPIC-inferred fractions of cancer-associated fibroblasts and endothelial cells (C).

Abbreviations: LUAD, lung adenocarcinoma; CAF, cancer-associated fibroblast

Supplementary Figure 2. Association of *TRIM29*-associated transcriptional module with stromal/immune features in the CPTAC-LUAD cohort. xCell-inferred stromal and endothelial populations (A); ESTIMATE scores (B); EPIC-inferred fractions of CAFs and endothelial cells (C).

Abbreviations: LUAD, lung adenocarcinoma; CAF, cancer-associated fibroblast

A

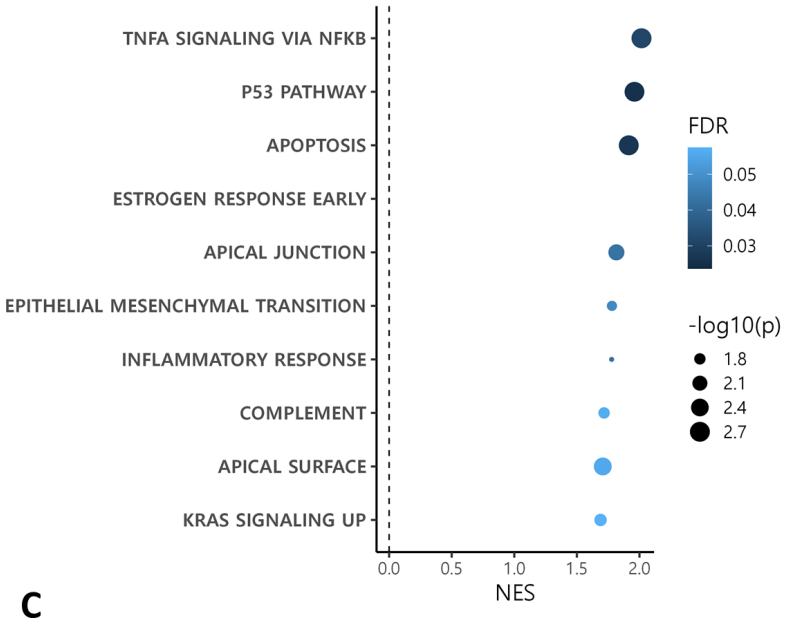

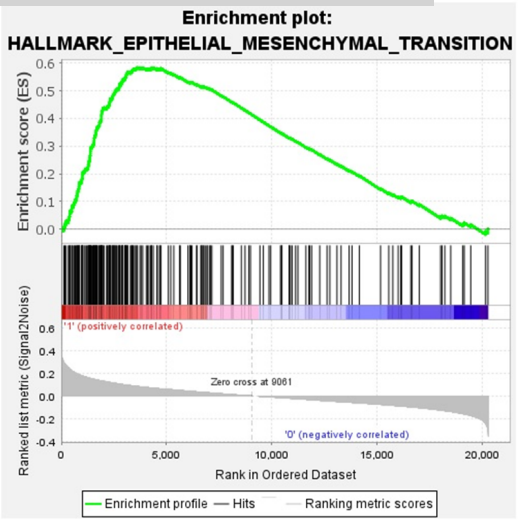

C

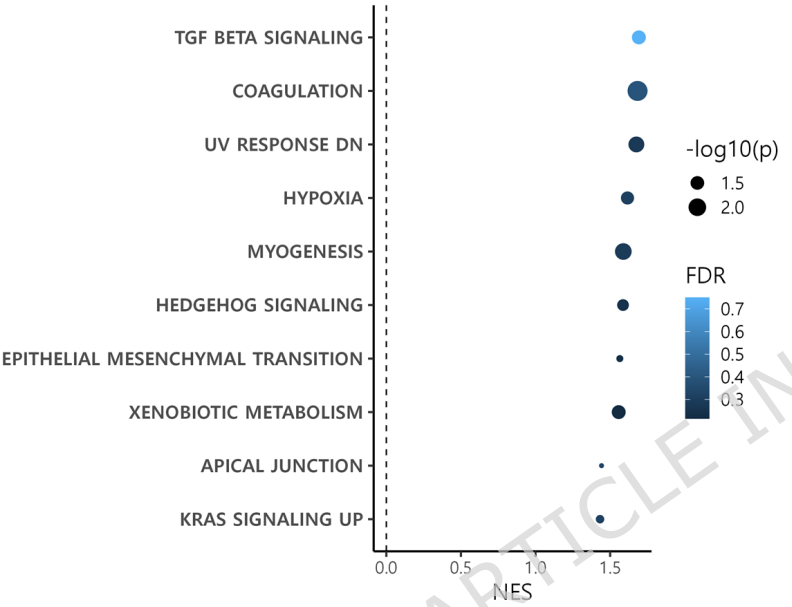

D

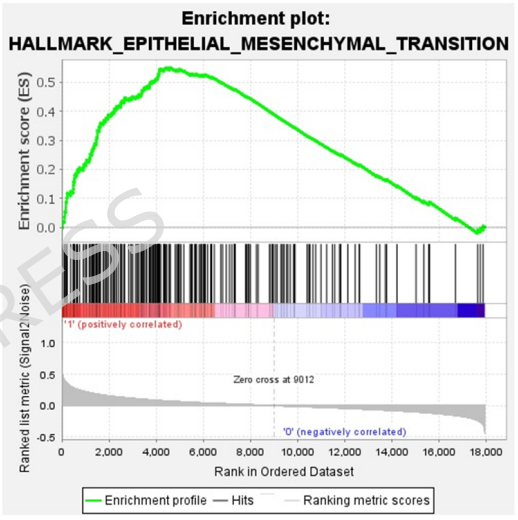

A xCell immune

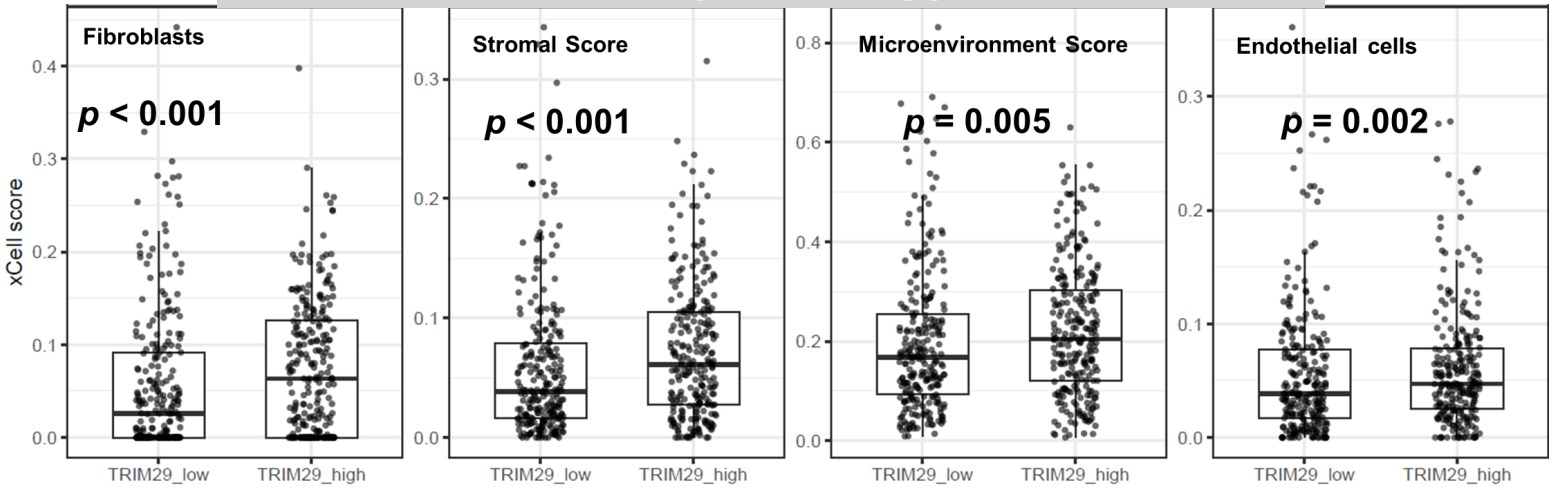

B ESTIMATE scores by *TRIM29* expression (TCGA LUAD, n=510)

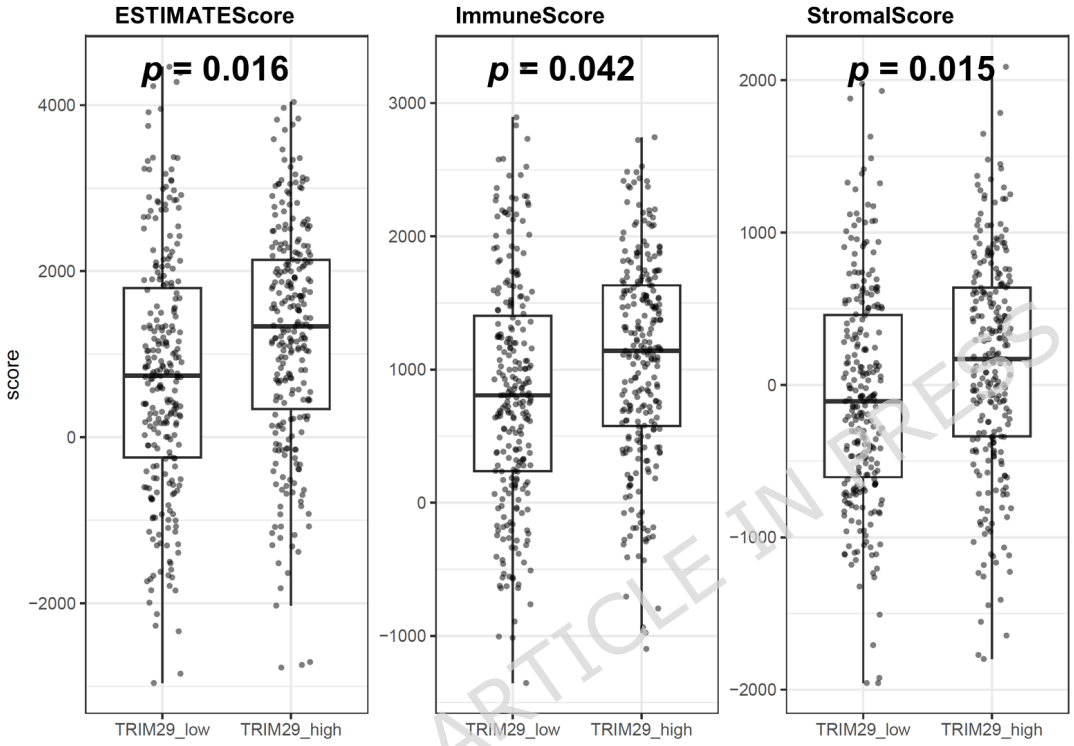

C EPIC fractions by *TRIM29* (TCGA LUAD, n=510)

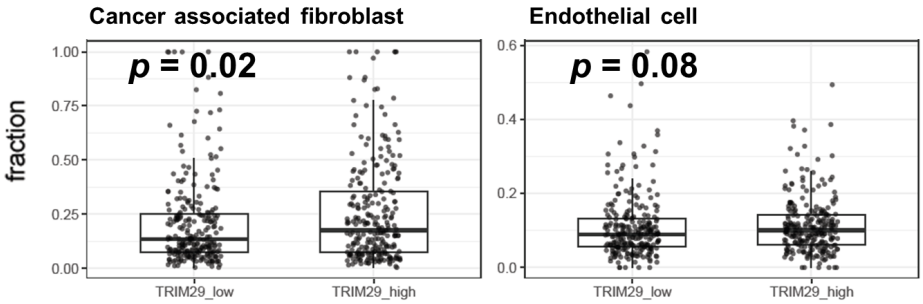

A xCell immune

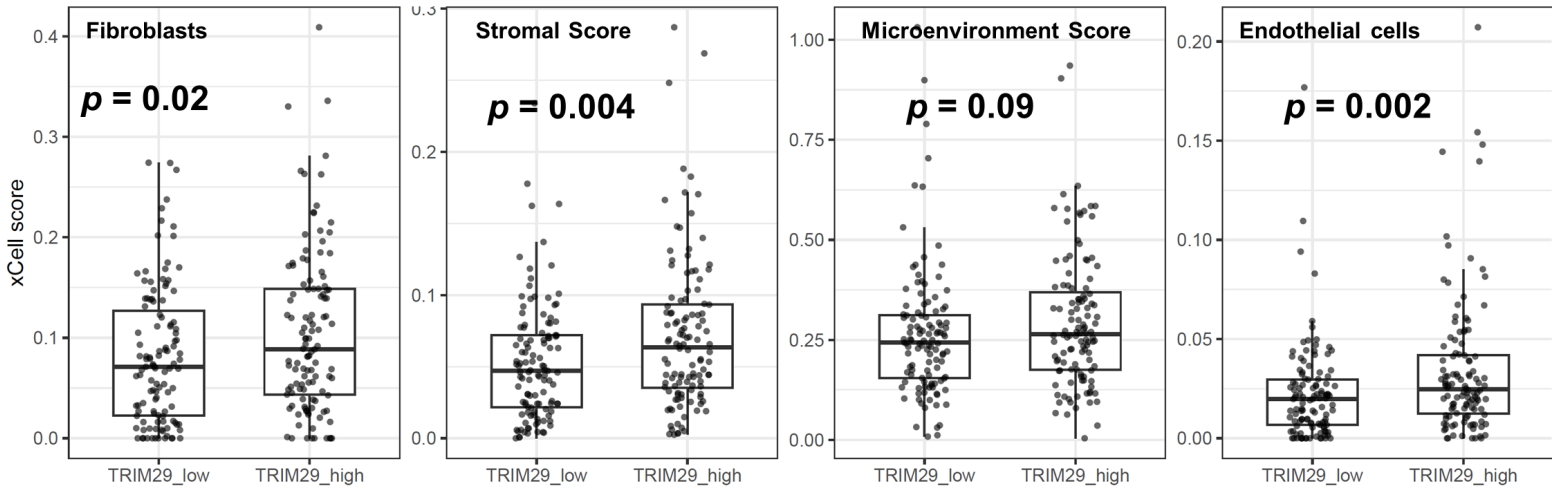

B ESTIMATE scores by *TRIM29* expression (CPTAC LUAD, n=110)

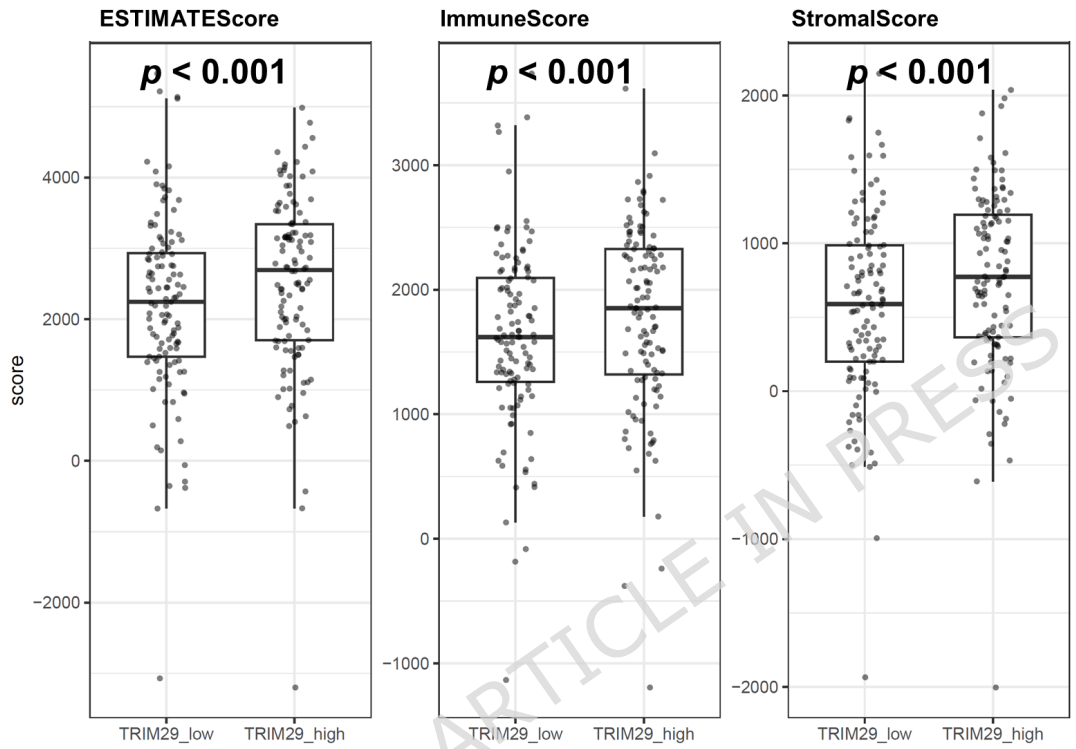

C EPIC fractions by *TRIM29* expression (CPTAC LUAD, n=110)

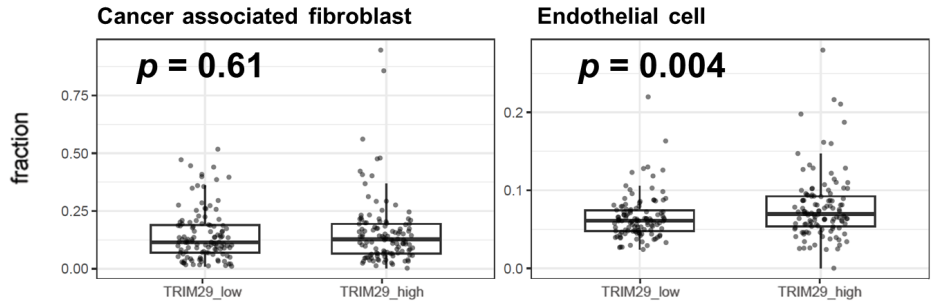

A TCGA (n=

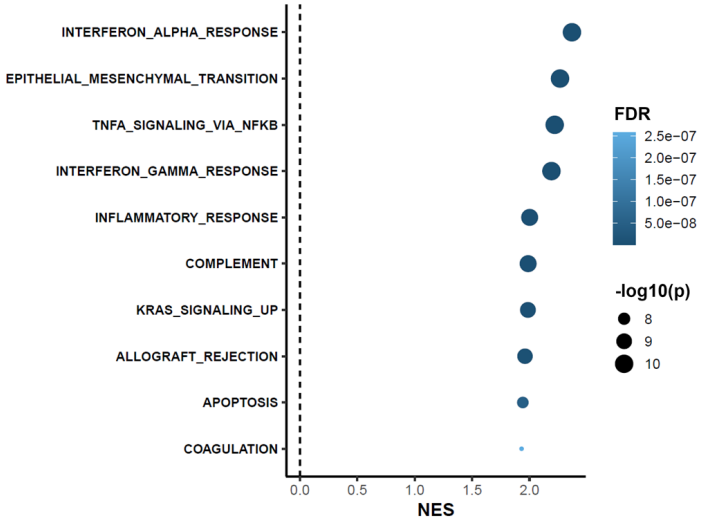

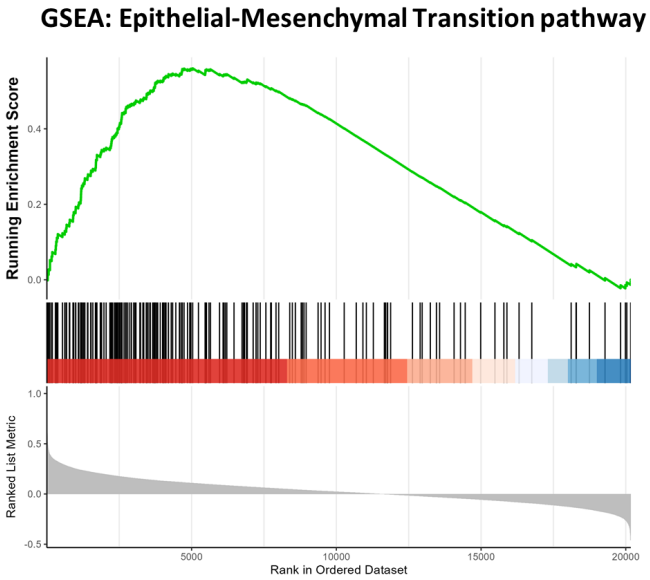

C CPTAC (n=110)

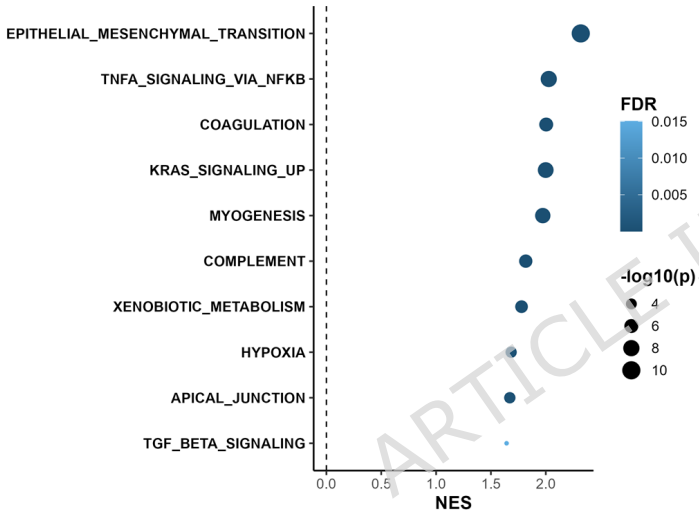

D

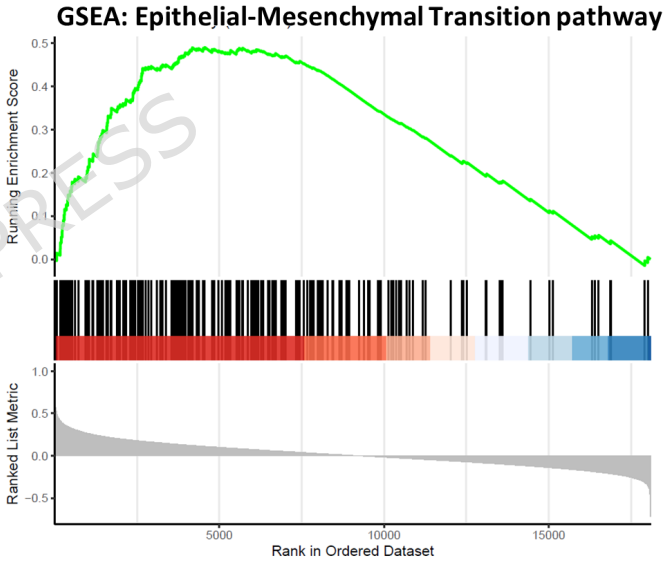

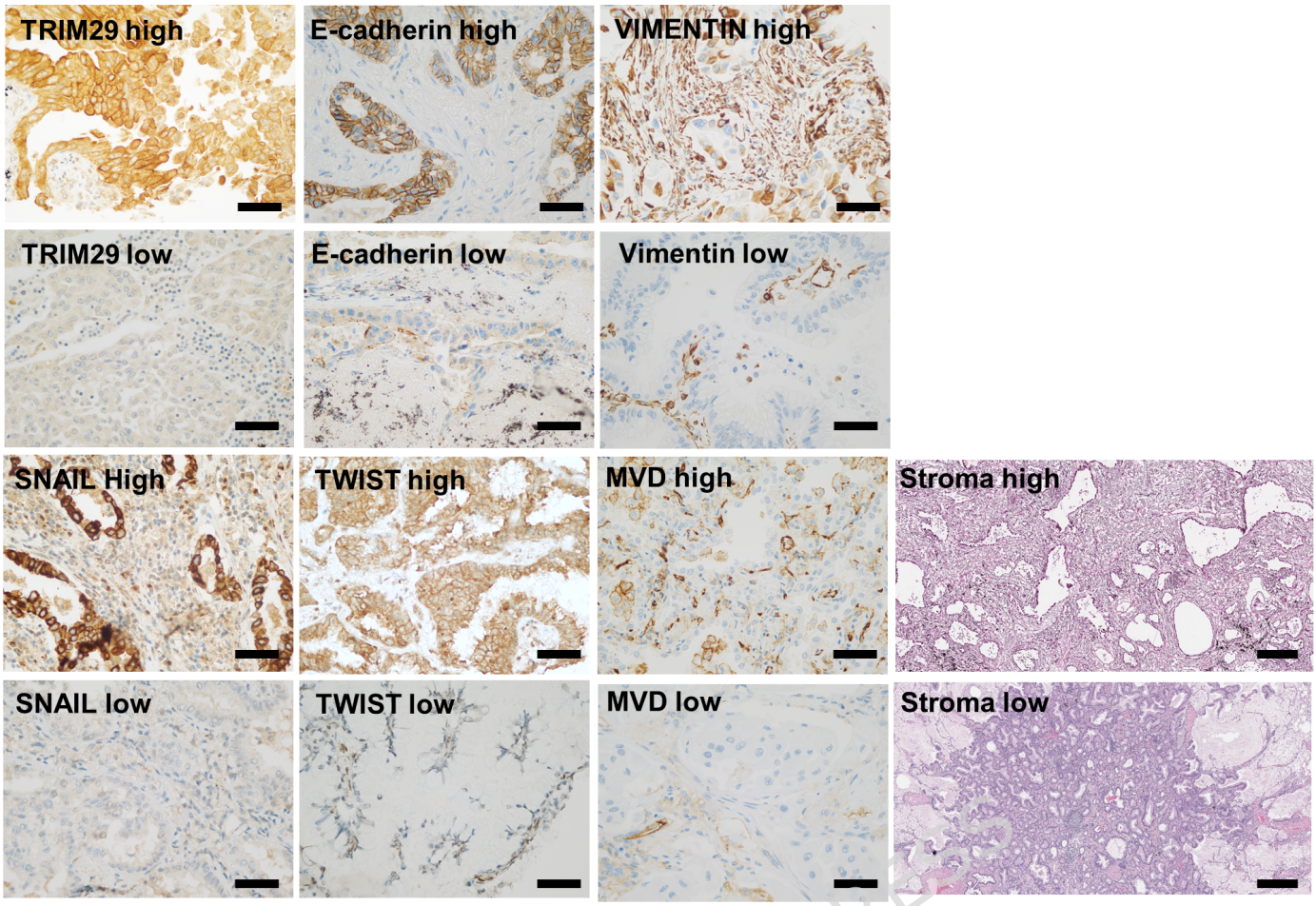

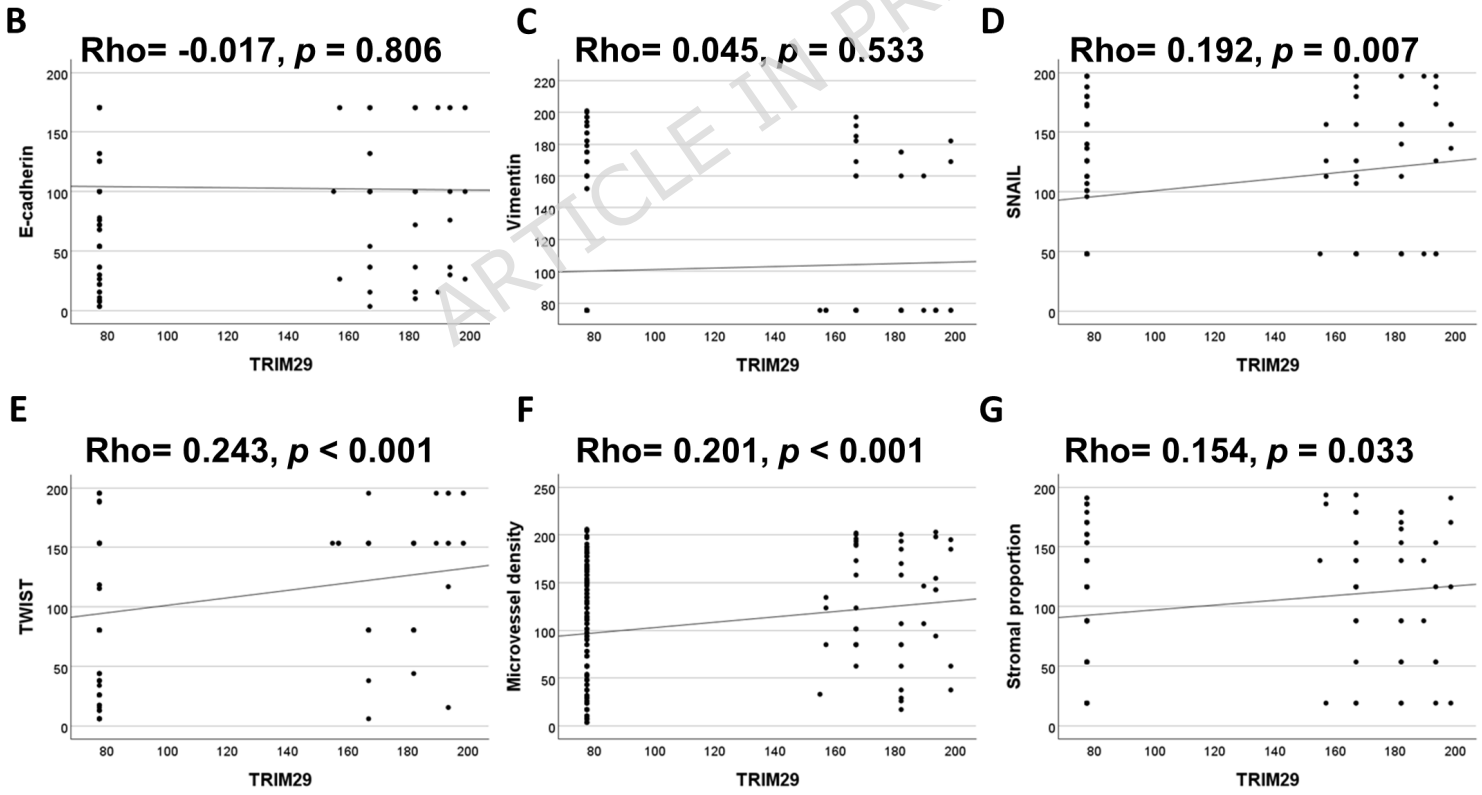

A KMplotter, N=1161

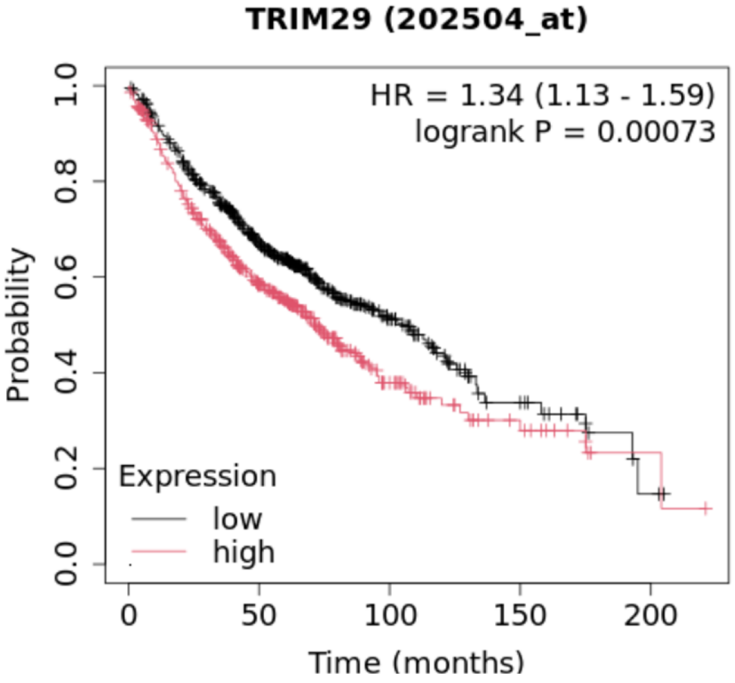

B Ajou University Hospital, N=200

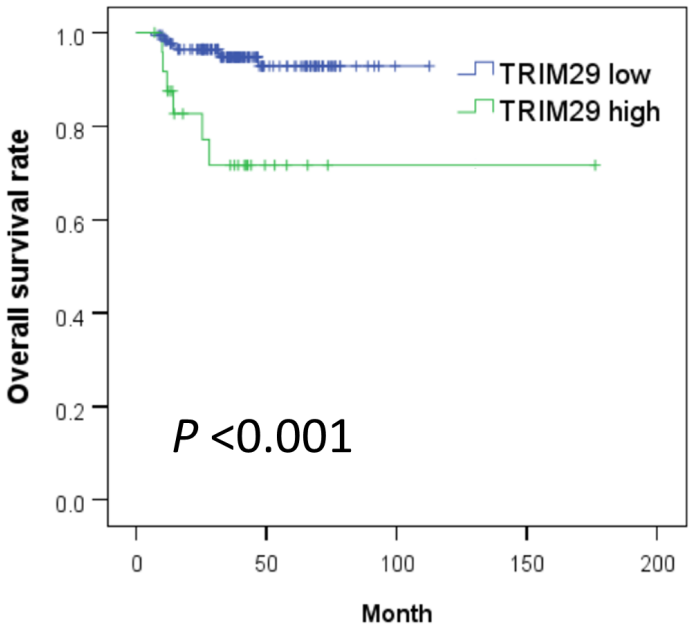

C Multivariate analysis

Covariate	HR	95% CI	P-value
TRIM29 (high vs. low)	3.061	1.011-9.263	0.048
Stage (III-IV vs. I-II)	4.805	1.667-13.846	0.004
Age (≥65 vs. <65)	3.534	0.946-13.207	0.061
Sex (male vs. female)	4.682	1.028-21.315	0.046

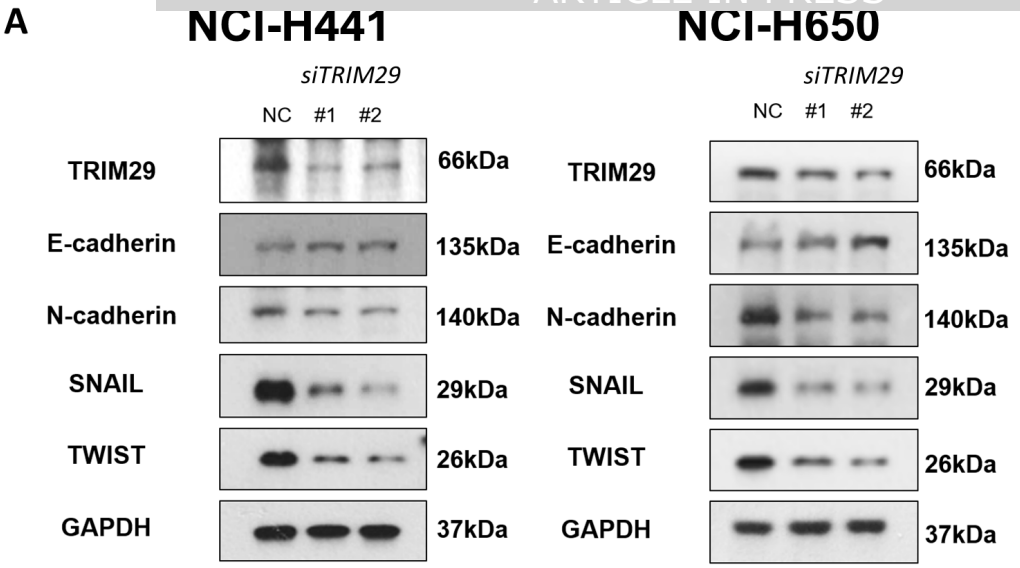

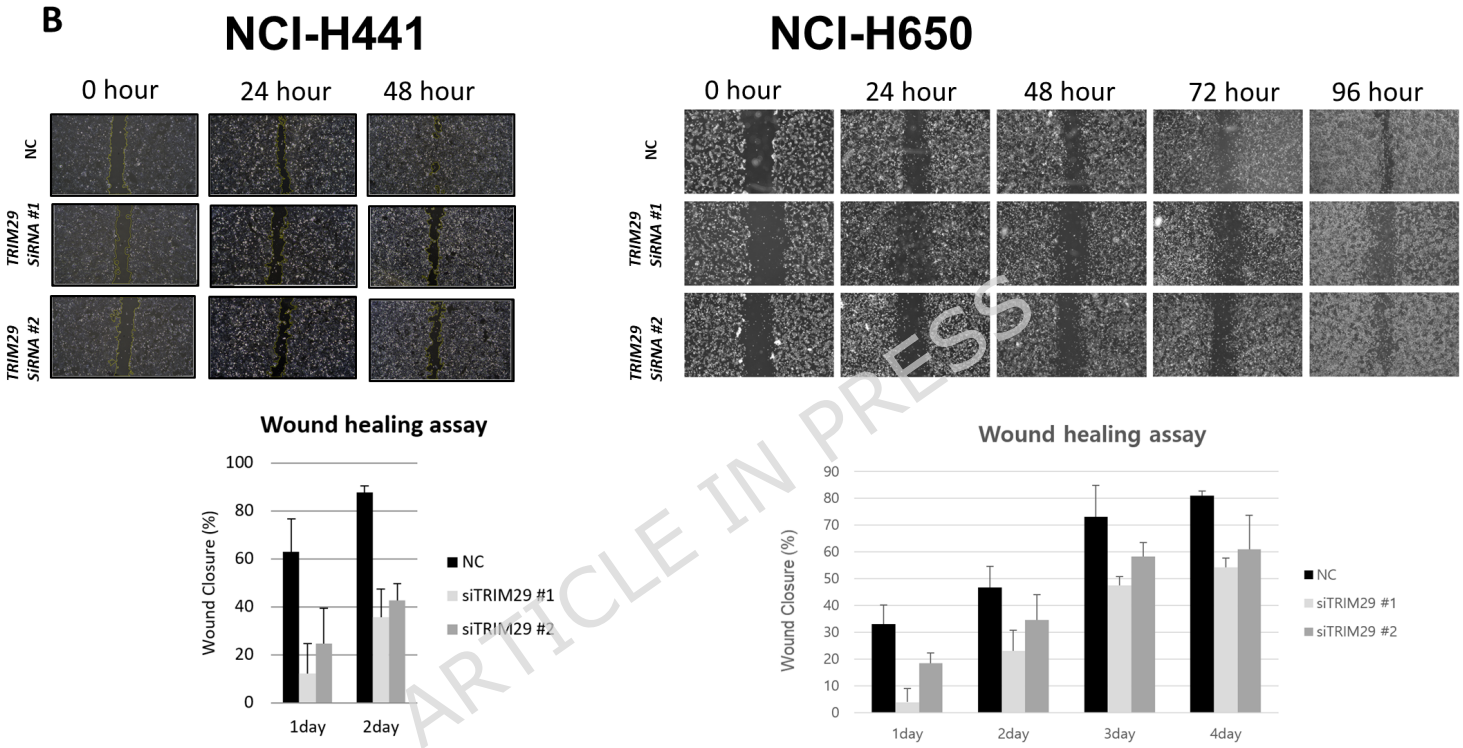

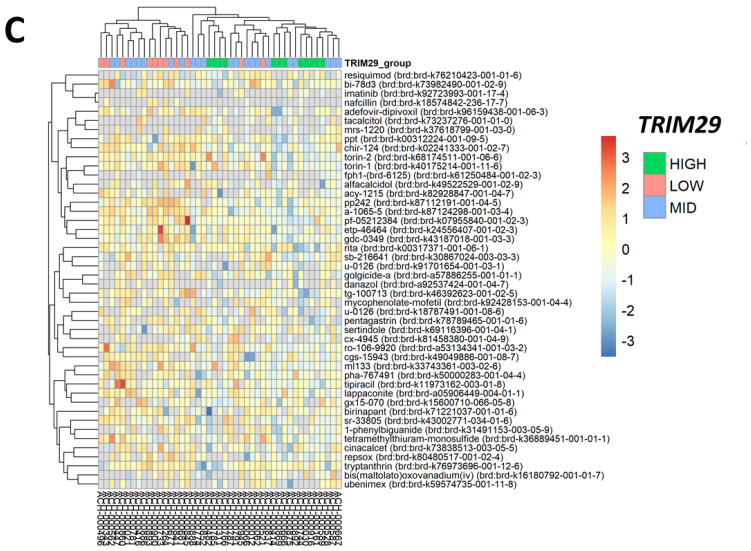

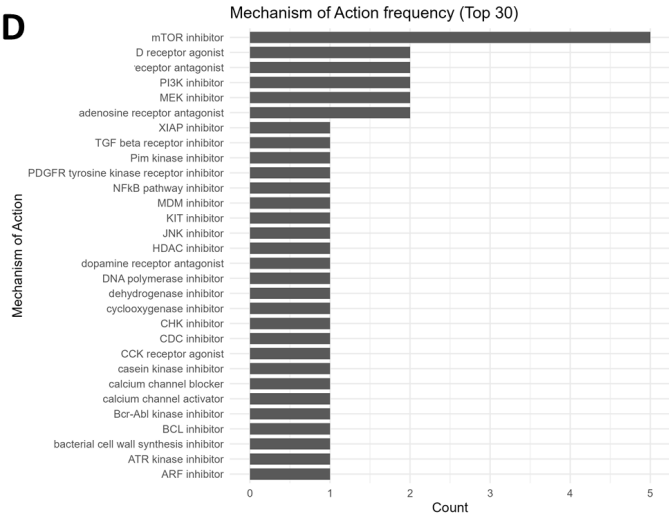

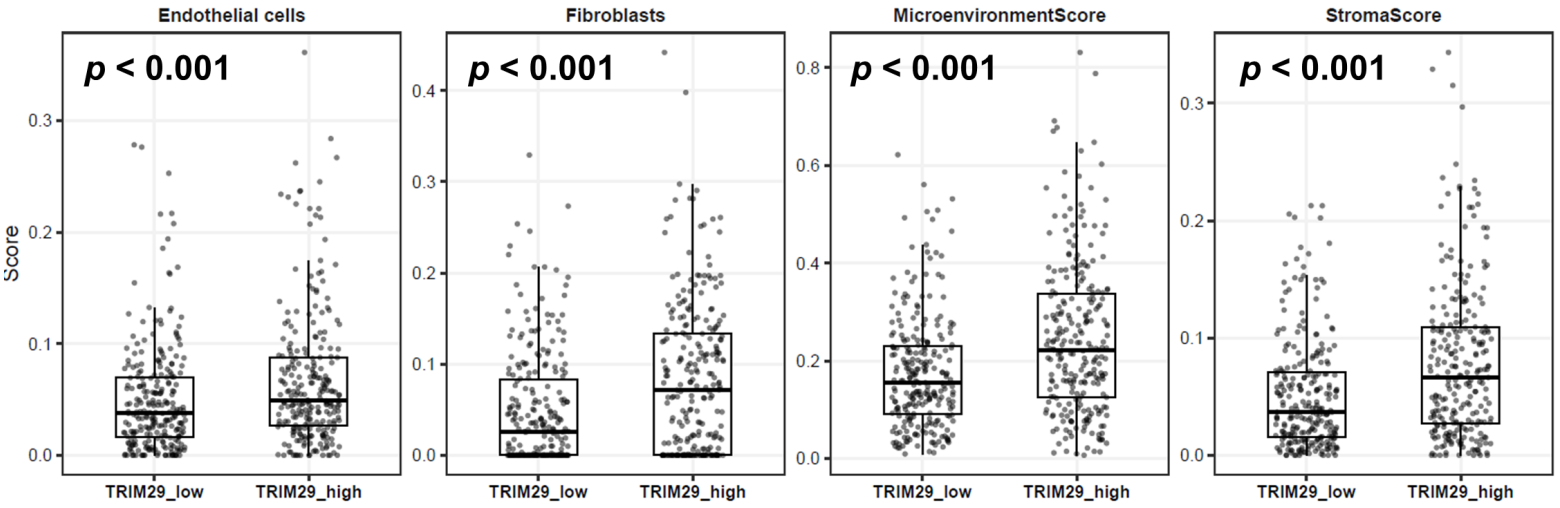

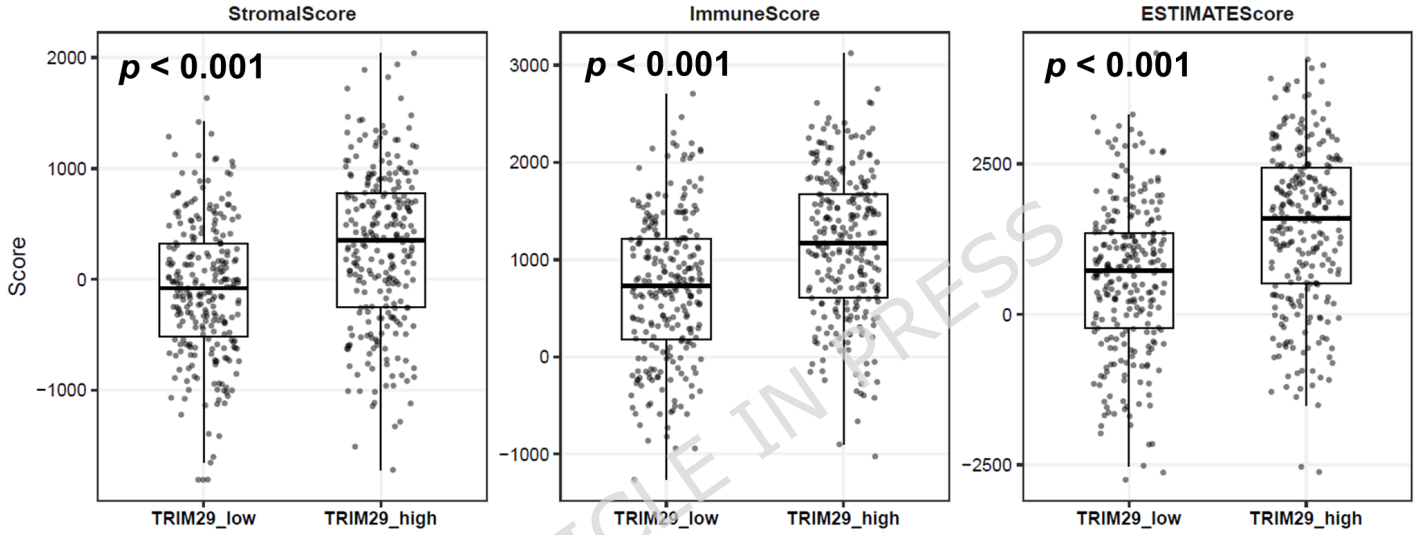

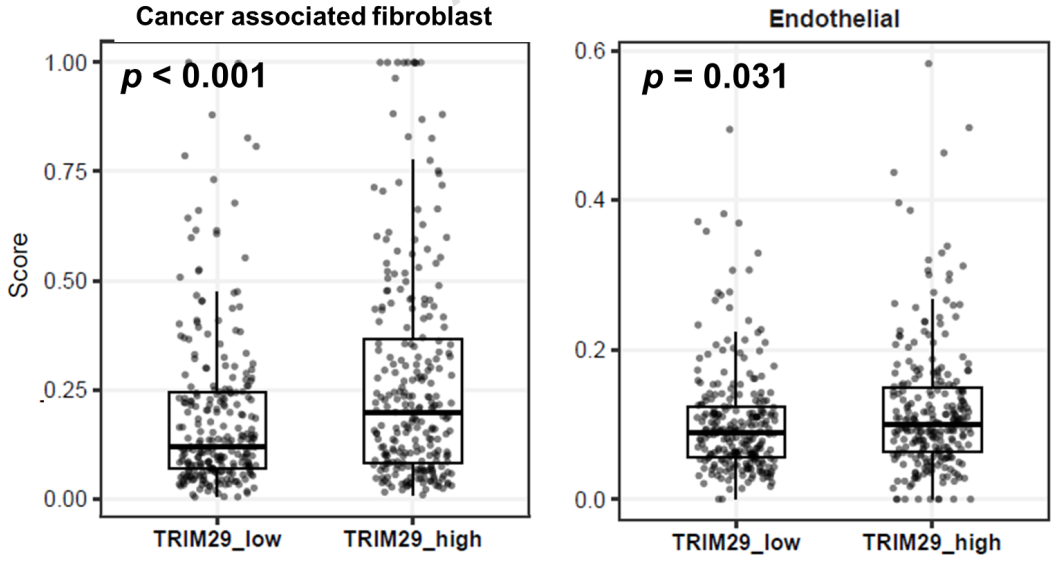

A xCell immune/stromal scores by *TRIM29* expression (CPTAC LUAD, n=110)

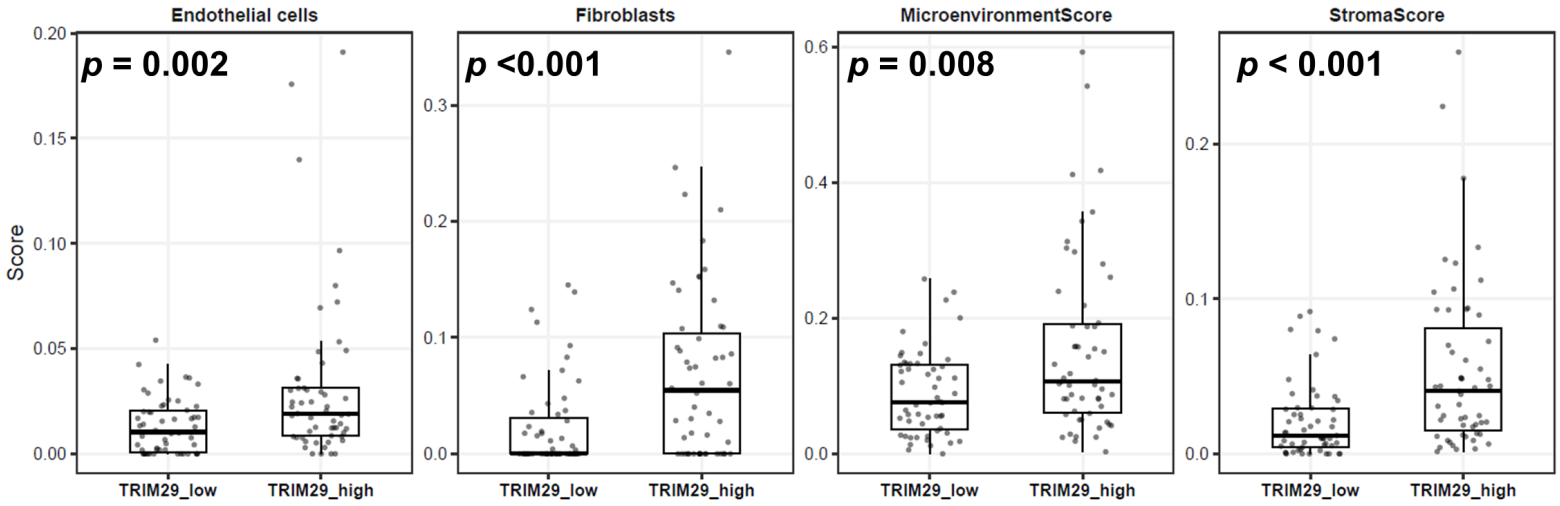

B ESTIMATE scores by *TRIM29* expression (CPTAC LUAD, n=110)

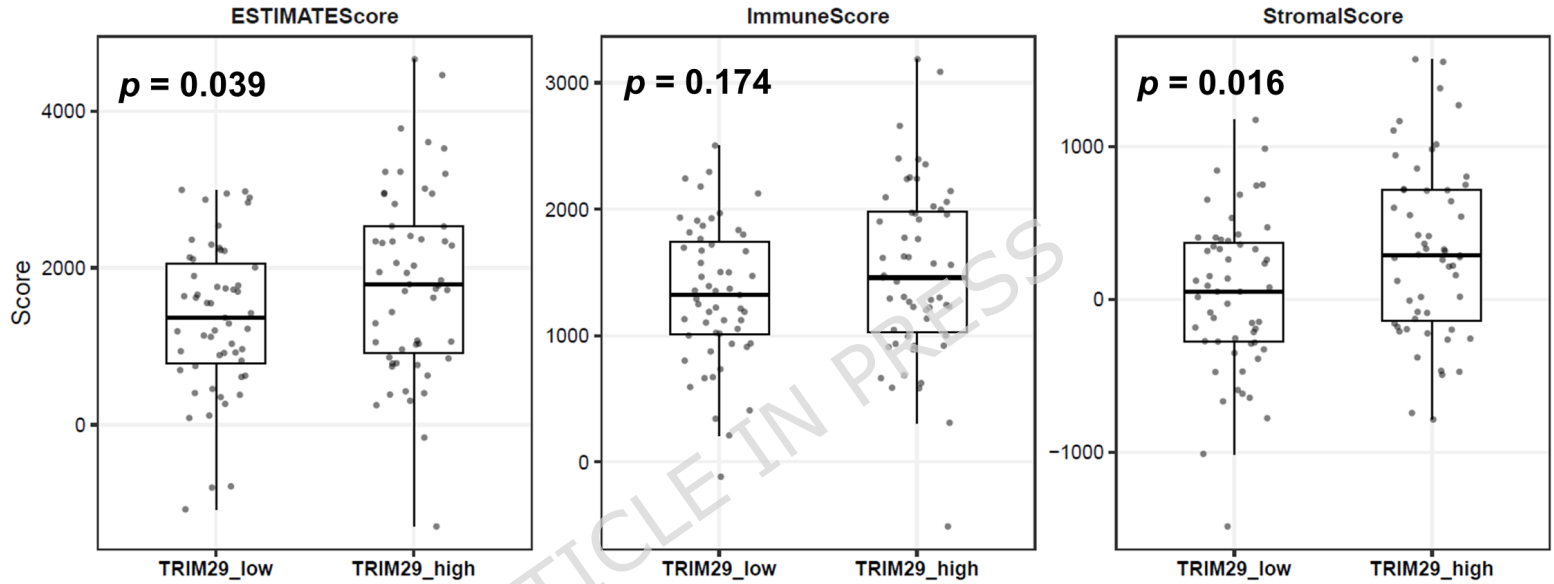

C EPIC fraction by *TRIM29* expression (CPTAC LUAD, n=110)